Considering syntrophic acetate oxidation and ionic strength improves the performance of models for food waste anaerobic digestion

Gabriel Capson-Tojo, Sergi Astals, Ángel Robles

Journal Pre-proofs

Considering syntrophic acetate oxidation and ionic strength improves the performance of models for food waste anaerobic digestion

Gabriel Capson-Tojo, Sergi Astals, Ángel Robles

PII: S0960-8524(21)01143-3
DOI: https://doi.org/10.1016/j.biortech.2021.125802
Reference: BITE 125802

To appear in: *Bioresource Technology*

Received Date: 8 July 2021
Revised Date: 12 August 2021
Accepted Date: 14 August 2021

Please cite this article as: Capson-Tojo, G., Astals, S., Robles, A., Considering syntrophic acetate oxidation and ionic strength improves the performance of models for food waste anaerobic digestion, *Bioresource Technology* (2021), doi: https://doi.org/10.1016/j.biortech.2021.125802

Considering syntrophic acetate oxidation and ionic strength improves the performance of models for food waste anaerobic digestion

Gabriel Capson-Tojo [a,b,*], Sergi Astals [c], Ángel Robles [d]

[a] Advanced Water Management Centre, The University of Queensland, Brisbane, QLD 4072, Australia (E-mail: *g.capsontojo@uq.edu.au*)

[b] CRETUS, Department of Chemical Engineering, Universidade de Santiago de Compostela, 15782 Santiago de Compostela, Galicia, Spain (E-mail: *gabriel.capson.tojo@usc.es*)

[c] Department of Chemical Engineering and Analytical Chemistry, University of Barcelona, C/Martí i Franquès 1, 08028 Barcelona, Spain (E-mail: *sastals@ub.edu*)

[d] Department of Chemical Engineering, Universitat de València, Avinguda de la Universitat s/n, 46100 Burjassot, València, Spain (E-mail: *angel.robles@uv.es*)

[*] Corresponding author: tel. +34 606.231.495, e-mail: *gabriel.capson.tojo@usc.es*

Abstract

Current mechanistic anaerobic digestion (AD) models cannot accurately represent the underlying processes occurring during food waste (FW) AD. This work presents an update of the Anaerobic Digestion Model no. 1 (ADM1) to provide accurate estimations of free ammonia concentrations and related inhibition thresholds, and model syntrophic acetate oxidation as acetate-consuming pathway. A modified Davies equation predicted NH_3 concentrations and pH more accurately, and better estimated associated inhibitory limits. Sensitivity analysis results showed the importance of accurate disintegration kinetics and volumetric mass transfer coefficients, as well as volatile fatty acids (VFAs) and hydrogen uptake rates. In contrast to the default ADM1, the modified ADM1 could represent methane production and VFA profiles simultaneously (particularly relevant for propionate uptake). The modified ADM1 was also

able to predict the predominant acetate-consuming and methane-producing microbial clades. Modelling results using data from reactors dosed with granular activated carbon showed that this additive improves hydrogen uptake.

Keywords

Anaerobic digestion; ADM1; Syntrophic acetate oxidation; Modelling; Ammonia inhibition

1. Introduction

Anaerobic digestion (AD) is a key technology for the sustainable management of several organic waste streams, including sewage sludge, food waste (FW), animal manure, agri-industrial waste, and industrial wastewater (Appels et al., 2008). AD is a multistage biochemical process that offers a triple role: (i) waste stabilization, (ii) production of renewable energy in the form of biogas, and (iii) nutrient recovery by digestate application. These benefits, together with new regulations penalizing cheaper alternatives (*i.e.* landfilling and incineration; European Directive 2018/850) and imposing circular economy action plans (European Commission Communication COM(2020)98), ensure a bright future for this biotechnology.

A clear example of the success of AD is the rapidly expanding treatment of concentrated wastes, such as FW or animal manure (Banks et al., 2008). The case of FW is particularly relevant, as its production is rapidly increasing due to population/economic growth, and policies imposing separate source selection and FW valorisation are being implemented (European Directive 2008/98/CE). These factors call for developing sustainable processes that can provide efficient FW valorisation, with AD standing among the most suitable options (Capson-Tojo et al., 2016).

AD mathematical modelling is well-stablished, and has largely been used for design purposes, operational analysis, technology development and process control (Regmi et al., 2019). The IWA Anaerobic Digestion Model no. 1 (ADM1), the most used AD model, is a mechanistic

model based on the underlying biological and physicochemical processes (Batstone et al., 2002; Weinrich and Nelles, 2021). The ADM1 was primarily developed to model sewage sludge AD in wastewater treatment plants. These digesters are characterised by relatively diluted solid concentrations (20-70 g $TS \cdot L^{-1}$; TS being total solids) and by relatively low risks of process inhibition and acidification (Appels et al., 2008; Astals et al., 2013). Accordingly, the default ADM1 is not able to accurately predict the performance of digesters treating concentrated organic streams or leading to high concentrations of inhibitors, such as ammonia. To overcome these limitations, several ADM1 modifications have been carried out in the last years. Relevant examples are the recent modifications of the ADM1 to consider variable mass/volume contents during high-solids AD (Pastor-Poquet et al., 2018), to account for non-ideal aqueous-phase chemistry (Patón et al., 2018; Solon et al., 2015), to include the syntrophic acetate oxidation (SAO) pathway (Montecchio et al., 2017; Rivera-Salvador et al., 2014), or to consider trace element (TE) complexation and precipitation (Flores-Alsina et al., 2016; Frunzo et al., 2019; Maharaj et al., 2019). As more research is carried out in AD, the knowledge on the underlying mechanisms governing the process increases, allowing to improve and modify models to accurately predict a broader spectrum of substrates, configurations, and operational conditions. A challenge in FW AD is free ammonia nitrogen (FAN) inhibition, caused by its high biodegradable protein concentrations and the low free water availability. High FAN concentrations cause inhibition of acetoclastic methanogenesis (AM; the predominant methane-producing pathway in digesters fed with sewage sludge). At FAN concentrations over 200-400 mg $FAN \cdot L^{-1}$, hydrogenotrophic methanogenesis (HM) becomes predominant (Banks et al., 2012), coupled with SAO (Jiang et al., 2017). This two-step methane production process relies on acetate oxidation to CO_2 and H_2 by SAO bacteria, followed by their conversion into methane by hydrogenotrophic archaea. This process is only thermodynamically favourable at low H_2 partial pressures (10-80 Pa), and constant H_2 removal by hydrogenotrophic archaea is crucial

for making SAO energetically feasible (Rivera-Salvador et al., 2014). SAO has been already included into the ADM1, improving the model accuracy in digesters treating poultry litter and pretreated waste sludge (Montecchio et al., 2017; Rivera-Salvador et al., 2014).

AD processes dominated by SAO and HM are known to be prone to propionic acid accumulation, a major inhibitor in AD reactors (Banks et al., 2012). Syntrophic propionate oxidation (SPO) also requires low H_2 partial pressures to be thermodynamically favourable, due to product-induced inhibition at high H_2 levels. For the same reason, SPO also depends on the concentrations of acetic acid (Batstone et al., 2002; Capson-Tojo et al., 2017). Therefore, AD instabilities leading to increases in the H_2 partial pressures can easily result in accumulation of acetic acid, which will further favour the accumulation of propionic acid. Because of its relevance, SPO is generally considered in mechanistic AD models (Batstone et al., 2002).

The high ionic strength in FW digesters causes another issue when considering traditional AD models, since the ion-pairing behaviour cannot be simplified to that of an ideal solution. Studies focusing on modelling ion speciation in concentrated AD systems have proved that assuming an ideal equilibrium can lead to overestimate FAN concentrations by up to 30% (Capson-Tojo et al., 2020; Hafner and Bisogni, 2009; Patón et al., 2018; Solon et al., 2015). Activity corrections have been applied to account for the effect of ionic strength on ion speciation, generally using the Davies equation for FAN quantification (Capson-Tojo et al., 2020; Patón et al., 2018; Solon et al., 2015). Despite its importance, this practice has been frequently omitted in the literature, even in publications devoted to FAN inhibition (Capson-Tojo et al., 2020; Rajagopal et al., 2013). FW digesters have the inherent risk of FAN inhibition and therefore a precise quantification of FAN is crucial to obtain coherent inhibitory limits that can be used to better predict process performance and inhibitory events (De Vrieze et al., 2015). The ADM1 does not include the SAO pathway nor the effect of the ionic strength on ion speciation. This limits its applicability for FW AD, particularly in dry systems. These limitations are particularly

relevant as full-scale dry digesters (treating undiluted substrates with TS contents over 15%) are becoming more common worldwide (Karthikeyan and Visvanathan, 2013; Motte et al., 2013).

Recent modelling efforts on FW AD modelling have improved the ADM1 performance (Montecchio et al., 2019; Poggio et al., 2016; Rathnasiri, 2016). However, to the best of our knowledge, no previous publication on FW AD has assessed the impact of including SAO and media ionic strength on the ADM1 performance. Zhao et al. (2019) modified the ADM1 to account for FW composition, and calibrated relevant parameters after a sensitivity analysis. They concluded that hydrolysis, disintegration, and acetate uptake were the most influential processes on methane production. Zhao et al. (2019) did not assess the importance of FAN inhibition. Poggio et al. (2016) proposed a substrate characterisation methodology based on substrate fractionation to enhance the ADM1 performance. Hydrolysis was also identified as a relevant kinetic process, and two particulate fractions were needed to accurately model FW AD (*i.e.* a readily and a slowly particulate biodegradable fraction). Poggio et al. (2016) concluded that their approach led to good predictions for methane yields and solid destruction, being less accurate for the prediction of methane flow rates, pH and VFA profiles. Rathnasiri (2016) applied the ADM1 after FW dilution with water, and Montecchio et al. (2019) for FW co-digestion with sewage sludge, a co-substrate with lower N concentration and higher water content. Both approaches reduced the impact of TAN concentration on the digester performance, which eased fitting the experimental results with the default ADM1. Indeed, Montecchio et al. (2019) stated that the ADM1 was only adequate for AD at high bacterial and methanogenic activities (achieved when co-digesting FW and sludge).

The main goal of this study was to design a modified ADM1 able to accurately simulate FW AD. The ADM1 was modified to consider: (i) SAO as acetate-consuming pathway, (ii) FAN estimation using the Davies equation (to account for non-ideal behaviour), and (iii)

methanogenic inhibition due to FAN using a threshold inhibition function (Astals et al., 2018). The modified and default ADM1s were compared, considering their ability to predict both the AD performances and the predominant microbial communities. The influence of AD additives (*e.g.* granular activated carbon (GAC)) on the resulting model parameters was also assessed.

2. Materials and methods

2.1. Inoculum source and substrate characteristics

The inoculum was collected from a territorial-industrial plant in the South of France treating a mixture of different organic streams at high total ammonia nitrogen (TAN) concentrations (7.3 ± 0.5 g $N \cdot L^{-1}$). FW was used as representative concentrated substrate. The FW was collected from different producers from the region of the Grand Narbonne (France). A proportional mixture (wet weight) of the different FWs was used as substrate. The characteristics of the FW and the inoculum, shown in Table 1, correspond to the average from two different FW sampling campaigns and to triplicate measurements for the inoculum.

2.2. Batch anaerobic digestion

Results from different sets of sequential batch digesters (with a working volume of 430 ± 2 mL) treating FW were used as input data to calibrate and validate the default and the modified ADM1s (Capson-Tojo et al., 2018a). Data from the 2nd feeding of the sequential batch reactors was used to ensure proper inoculum adaptation and reactor operation. The digesters (in triplicate) were started with 60 g of FW as substrate (raw) at a substrate to inoculum ratio of 1 g $VS \cdot g\ VS^{-1}$ (with resulting FW concentrations of around 30 g VS $FW \cdot L^{-1}$; VS being volatile solids). The reactors were incubated at 37 ± 0.2 °C. The incubation system was an Automated Methane Potential Testing System (AMPTSII) (Bioprocess Control, Sweden) consisting of 15 parallel reactors with a total volume of 500 mL (of which 12 were used). To determine the methane flow rate, the headspace of each rector was connected to a carbon dioxide trap (NaOH

5% solution) and then to a gas flow meter. The reactors were automatically stirred for 1 minute every 10 minutes at 40 rpm. Before starting the incubation, the headspace was flushed with pure N_2 to ensure anaerobic conditions. To account for endogenous respiration, a blank reactor containing only inoculum was also run (in triplicate). The methane production from the blank was subtracted from the biogas produced by the reactors fed with FW. The batches were stopped after 34 days, once the biogas production stopped in all reactors, and the total volatile fatty acids (VFAs) concentration was assumed to be negligible.

To assess the applicability of the proposed model modifications, data from reactors working under different conditions were used: (i) control conditions (solely fed with FW), and (ii) supplemented with GAC (dosed at 10 $g \cdot L^{-1}$). A detailed explanation of the experimental design and the sampling procedure can be found in Capson-Tojo et al. (2018a).

2.3. Analytical methods

2.3.1. Physicochemical characterization of the FW

TS and VS contents were measured according to the standard methods of the American Public Health Association (APHA, 2017). Carbohydrate contents were determined using the Dubois method (Dubois et al., 1956), and lipid contents via accelerated solvent extraction using an ASE®200, DIONEX (California, United States of America) coupled to a MULTIVAPOR P-12, BUCHI (Aquon, Netherlands) with heptane as solvent (100 bar, 105 °C, 5 cycles of 10 min static and 100 s purge) (APHA, 2017). Total Kjeldahl Nitrogen (TKN) contents were determined with an AutoKjehdahl Unit K-370, BUCHI, and the protein contents were estimated from TKN values using a factor of 6.25 g protein·g organic N^{-1} (Galí et al., 2009). The pH was measured using a WTW (London, United Kingdom) pHmeter series inoLab pH720. The FW biochemical methane potential (BMP) was determined according to Motte et al. (2014), following Angelidaki et al. (2009). The chemical oxygen demand (COD) content of the FW was estimated from the contents in carbohydrates (1.19 g $COD \cdot g^{-1}$), proteins (1.42 g $COD \cdot g^{-1}$)

and lipids (2.90 g COD·g^{-1}), assuming a 10% of inert COD (based on Batstone et al., (2002), and from the FW biodegradability estimated from the BMPs, of 92%).

2.3.2. Analysis of metabolites, final products, and microbial communities

A plastic tube connected to the cover of each AMPTSII reactor enabled digestate sampling without modifying the composition of the gas in the headspace. Samples (5-10 mL) were taken approximately every 2 days, with a total of 15 samples per reactor taken during the duration of the experiments. The concentrations of volatile fatty acids (VFAs) and ionic species (*i.e.* TAN, PO_4^{3-}, Na^+, or K^+) in the digestates were analysed by gas and ion chromatography, as described in Motte et al. (2013). The product yields were corrected to account for the digestate removed, by accounting for the mass of substrate removed in every sampling.

The methane flow rates were quantified using CO_2 traps and gas flow meters connected to the headspace of the reactors. The microbial communities at the beginning and the end of the tests were analysed via 16S rRNA sequencing (MiSeq), as described in Moscoviz et al. (2017).

2.4. ADM1 modifications

2.4.1. Syntrophic acetate oxidation

SAO was included into the ADM1 following a similar approach to that presented in Rivera-Salvador et al. (2014). Stoichiometry was set according to Equation 1, and Monod kinetics were applied for SAO. As in Rivera-Salvador et al. (2014), hydrogen inhibition in acetate uptake by SAO was considered using a non-competitive inhibition function.

$$CH_3COO^- + 4H_2O \rightarrow 2HCO_3^- + H^+ + 4H_2\ (g) \qquad \Delta G'^\circ = +\ 104\ kJ\cdot mol^{-1} \qquad \text{Eq.1}$$

2.4.2. FAN quantification using a modified Davies equation

The FAN concentrations were calculated using the modified Davies equation proposed in Capson-Tojo et al. (2020). This approach considers the pH, temperature and I of the media, introducing an activity coefficient (*f*) as correction factor into the ideal equilibrium equation, resulting in Equation 2 (Stumm and Morgan, 1996). The set of expressions used is as follows:

$$FAN = \frac{K_a \cdot f \cdot TAN}{K_a \cdot f + 10^{-pH}} \quad \text{Eq. 2}$$

$$f = 10^{\left(-A \cdot z_i^2 \cdot \left(\left(\frac{\sqrt{I}}{1+\sqrt{I}}\right) - \lambda \cdot I\right)\right)} \quad \text{Eq. 3}$$

$$A = 1.82 \cdot 10^6 \cdot (\varepsilon \cdot T)^{-\frac{3}{2}} \quad \text{Eq. 4}$$

$$I = \frac{1}{2} \sum_{i=1}^{n} C_i \cdot z_i^2 \quad \text{Eq. 5}$$

Where K_a is the acid-base equilibrium constant, I is the ionic strength (M), λ is an empirically determined constant (0.1276 according to Capson-Tojo et al. (2020)), ε is the dielectric constant of water at the working temperature (74.828 and 68.345 at 35 and 55 ºC, respectively), C_i is the concentration of the species i (M), T is the temperature, and z_i is the corresponding charge.

2.4.3. FAN threshold inhibition function

The inhibition function considered for FAN inhibition on methanogenic archaea was the threshold inhibition function proposed by Astals et al. (2018):

$$I_{FAN} = \begin{cases} 0 & ;\ if\ FAN \leq K_{I,NH3,min} \\ 1 - e^{-2.77259\left(\frac{(FAN - K_{I,NH3,min})}{(K_{I,NH3,max} - K_{I,NH3,min})}\right)^2} & ;\ if\ FAN > K_{I,NH3,min} \end{cases} \quad \text{Eq. 6}$$

Where I_{FAN} is the inhibition factor related to the presence of FAN, $K_{I,NH3,min}$ and $K_{I,NH3,max}$ are the FAN concentrations where inhibition starts (onset concentration) and when it is almost complete (specific methanogenic activity (SMA) = $0.06 \cdot SMA_{max}$), respectively (Astals et al., 2018). The constant 2.77259 ensures that the midpoint between $K_{I,NH3,min}$ and $K_{I,NH3,max}$ equals $K_{I,NH3}$ (FAN 50% inhibitory concentration for acetate uptake by methanogens).

The threshold function provides a more accurate representation of the impact of FAN on AM activity, and it allows to identify a lower and an upper inhibition limit (Astals et al., 2018). This inhibition function allows defining precise thresholds that can serve to simulate changes in the predominant methanogenic pathways according to the FAN concentrations.

2.4.4. Accounting for the different dynamics of butyrate and valerate consumption

The modified ADM1 uncoupled the uptake of butyrate and valerate by adding a new bacterial group responsible for valerate uptake (X_{c5}). In this approach, X_{c4} were only responsible for the uptake of butyrate (opposed to the ADM1, where X_{c4} consume both butyrate and valerate). The competitive term originally present in the default ADM1 was removed in the rate equations for butyrate and valerate uptake. This approach was implemented in previous models also dealing with high-solids AD, aiming at obtaining an accurate representation of the different kinetics of butyrate and valerate uptake (Pastor-Poquet et al., 2019, 2018).

2.5. Model calibration and evaluation

To compare the models (*i.e.* default *vs.* modified ADM1s) and to evaluate the effects of GAC on the AD performance (see Section 2.2), a systematic approach was followed. First, a global sensitivity analysis (GSA) was carried out for each model to identify influential parameters on the model outputs. Afterwards, these parameters were dynamically calibrated to improve the prediction capabilities of the models and to compare between the different experimental conditions (*i.e.* control *vs.* GAC-dosed reactors). The required stoichiometric parameters, biomass compositions, biomass yields, and physicochemical parameters were all obtained from the literature, as well as the initial values of the kinetic parameters (Batstone et al., 2002; Capson-Tojo et al., 2020; Rivera-Salvador et al., 2014; Rosen and Jeppsson, 2006). We are willing to share the code files corresponding to both the default and the modified ADM1s (implemented in MATLAB® (MATLAB R2021a, The MathWorks Inc., Natick, MA, USA)).

2.5.1. Sensitivity analysis

The GSA methodology implemented was similar to the one described in Robles et al. (2014), based on the Morris screening Method (Morris, 1991). This approach consists in a one-factor-at-a-time method of GSA, which evaluates the distribution of the scaled elementary effects of each input factor (model parameters) upon model outputs (methane production rates and VFAs concentration), which is afterwards used to calculate the statistical parameters that provide

sensitivity data. The variation for each input factor was set to ±20% of the default value, through a resolution of 4 *p* levels. The number of evaluated trajectories was 100. The absolute mean (μ^*) and the standard deviation (σ) of the scaled elementary effects of each distribution were used as sensitivity measures (Campolongo et al., 2007). The graphical Morris approach was used to systematically differentiate between input factors that could significantly influence the model. The μ^* and σ obtained for all the scaled elementary effects of each distribution were plotted. Factors with high μ^* and (relatively) small σ were considered to be influential, with linear and additive effects on the outputs. Factors with small μ^* but high σ were considered to be influential, with non-linear or interactive effects on the outputs. Factors with low μ and σ were considered as non-influential (Morris, 1991).

2.5.2. Dynamic calibration of the model

The parameters considered as influential from the GSA results were dynamically calibrated by adjusting the relevant simulated data (*i.e.* methane production rates and VFA concentrations) to the experimental results. A global constrained optimization was conducted using a genetic algorithm (MATLAB R2021a). Bound constrains for variations of model inputs were set to ±95% of default values, except for pH-related inhibition parameters (±10%). The objective function to be minimised (standardized residuals) is shown in Eq. 7, where X_{SIM} and X_{EXP} are the simulated and measured values for each variable *i*. No ponderation factors were applied.

$$\sum_{i=1}^{n}\left(\sum\frac{\left|X_{SIM_i}-X_{EXP_i}\right|}{\sqrt{\mathrm{std}\left(X_{EXP_i}\right)}}\right) \quad \text{(Eq. 7)}$$

3. Results and discussion

3.1. Comparison of the resulting models after sensitivity analysis and calibration

3.1.1. Results from global sensitivity analysis

The graphical outputs from the GSA for both the default and the modified ADM1 for the control

reactor are shown in Fig. 1. Regarding the methane production rates (Q_{CH4}), the results of both models (Figs. 1A and 1F) showed that the most relevant parameters were all related to acetate uptake (*e.g.* AM or SAO maximum specific uptake rates (k_m), and AM inhibition parameters, either $K_{I,NH3}$ or $K_{I,NH3,max,acet}$ ($K_{I,NH3,max}$ for acetotrophs) depending on the model). The disintegration and decay first order rate constants (k_{dis} and k_{dec}) and the volumetric mass transfer coefficient (k_La) also appeared as relevant. The acetate-uptake related parameters (*i.e.* $k_{m,ac}$ and $k_{m,SAO}$) illustrate the predominance of this VFA as main methane-producing intermediate metabolite, which is in agreement with FW AD literature (Capson-Tojo et al., 2017; Jiang et al., 2017). The relevance of k_{dis} and k_La is explained by the high contents of solids in the reactors (the high TS contents in FW, around 20%, often lead to TS contents of 5%). With most of the organic matter being present as particles, their disintegration appears as a critical process, potentially acting as rate limiting step. Furthermore, the high TS contents and consequent lack of water also affect gas transfer and diffusion, reason why the k_La is important.

The model structure also affected the results, with SAO-related parameters (*i.e.* $k_{m,SAO}$) appearing as relevant in the modified ADM1. Both models showed again similar results regarding the uptake of acetate (Figs. 1B and 1G), with parameters related to acetate uptake being deemed as relevant (AM or SAO uptake kinetic parameters, or AM inhibition parameters). SAO-related parameters were also relevant in the modified ADM1, confirming the importance of this pathway. The uptake of other VFAs (*i.e.* propionate, butyrate, and valerate; Figs. 1C-E and 1H-J) was governed by the respective Monod kinetic parameters (*i.e.* corresponding k_m and K_S; K_S being the saturation constant) and by parameters related to hydrogen uptake (*e.g.* hydrogen uptake parameters and corresponding inhibitory terms for each VFA). In the modified ADM1, k_{dis} was also found relevant, due to the solid nature of FW.

3.1.2. Model calibration and comparison of prediction capabilities: default vs. modified ADM1

The parameters deemed as relevant according to the GSA were calibrated using both models

297 and the control reactor dataset (as in Section 3.1.1). The GSA allowed to reduce the number of
298 parameters to calibrate from an initial set of 31 in the default ADM1 and 41 in the modified
299 ADM1, to 13 and 16, respectively. The calibration results are shown in Table 2.
300 The parameters deemed as relevant for methane production and/or VFA uptake were selected
301 for calibration. Despite the influence of $pH_{UL,ac}$ (pH upper limit for acetotrophs) on the resulting
302 methane flow rates and acetate uptake rates (see Fig. 1), $pH_{UL,ac}$ and $pH_{LL,ac}$ (pH lower limit for
303 acetotrophs) were excluded from the calibration of the modified ADM1. pH-related inhibition
304 parameters were deemed as relevant by the GSA because, mathematically, AM can be inhibited
305 by modifying the pH inhibition limits. Nevertheless, the resulting calibrated values leading to
306 AM inhibition by pH were 8.0-8.5 for $pH_{LL,ac}$ and over 9.0 for $pH_{UL,ac}$, which biologically do
307 not make sense (Batstone et al., 2002). Therefore, including these parameters in the calibration
308 procedure resulted in illogical inhibition limits, affecting the values of other parameters and
309 leading to inaccurate results. Furthermore, using the default ADM1, the calibrated values for
310 $pH_{UL,ac}$ were 6.4-7.1, which agree with values reported in the literature (Batstone et al., 2002).
311 The calibration results showed that FW has a relatively fast disintegration kinetics (>0.6 d^{-1})
312 compared to other solid substrates, with values of k_{dis} higher than those reported in the literature
313 (*e.g.* 0.24 d^{-1} for cattle manure or 0.10 d^{-1} for pig manure (Batstone et al., 2002)). This result is
314 in agreement with the well-known faster disintegration and hydrolysis of FW (Koch et al.,
315 2015). The much lower values of k_La when compared to the literature are related to the lack of
316 water and the inherent difficult mixing at high solid contents.
317 To understand the resulting values of the kinetic parameters for each model, their prediction
318 performances and the predicted dominant pathways must be analysed in detail. The modelling
319 results are presented in Fig. 2 (methane flow rates and VFA profiles) and Fig. 3 (biomass
320 concentrations, and pH and TAN/FAN concentrations). As shown in Fig. 2, while both models
321 represented accurately the acetate and total VFA profiles (parity plots with R^2 of 0.98-0.99),

the calibrated default ADM1 was not able to represent the methane production rate (R^2 of 0.61) nor the final consumption of propionate (see Fig. 2). In contrast, the modified ADM1 provided more accurate predictions in both cases (R^2 of 0.94 and 0.99, respectively).

The improved predicting capabilities of the modified ADM1 are related to the underlying processes governing AD in each model. In the default ADM1, AM is the only acetate-consuming pathway available. Therefore, to fit the experimental methane production rates and the total VFA and acetate profiles, the FAN inhibitory concentrations for acetoclastic archaea ($K_{I,NH3}$) need to be far above commonly applied inhibitory concentrations (*e.g.* $K_{I,NH3}$ values of at 0.0030 *vs.* 0.0018 M (Batstone et al., 2002)). In contrast, the calibration results with the modified ADM1 showed a realistic FAN inhibitory limit for acetoclastic archaea (*i.e.* a $K_{I,NH3,max,acet}$ of 0.011 M, as in Capson-Tojo et al. (2020)). This value led to inhibition of AM, which can be confirmed when looking at the predicted concentrations of methanogenic archaea (Fig. 3). Therefore, SAO was the main acetate-consuming pathway, and HM the main methane-producing one, which is in agreement with the experimental results (where the presence of acetoclastic archaea at the end of the batch tests was negligible, see Capson-Tojo et al. (2018a) for a detailed discussion on the microbial communities in the reactors). The accurate representation of the underlying microbial processes by the modified ADM1 was facilitated by including SAO as metabolic pathway, and by using realistic FAN inhibitory limits for acetoclastic archaea. These allowed to account for the observed AM inhibition, resulting in the dominance of SAO (and HM) despite their slower overall kinetics. The low concentrations of syntrophic bacteria predicted by the modified ADM1 are caused by their slow growth, generally representing a minor part of the total microbial community in digesters (Hao et al., 2020). These results agree with previous studies dealing with SAO during AD at high N concentrations. Hydrogenotrophic methanogens were also dominant in thermophilic AD of poultry litter (Rivera-Salvador et al., 2014), and Montecchio et al. (2017) did not detect any acetoclastic

archaea in their reactors treating sludge at 0.3 g FAN·L^{-1}.

The different predominant methanogenic pathways between both models explain the inability of the default ADM1 to predict the methane production rates. The high H_2 concentrations occurring during FW AD can potentially make thermodynamically unfavourable the processes in which H_2 was produced, such as SAO, propionate oxidation, butyrate oxidation, and valerate oxidation (accounted for in both models by the 50% inhibitory concentrations of H_2, $K_{I,h2,j}$). This can lead to the accumulation of VFAs often seen in full-scale FW digesters (Banks et al., 2012; Capson-Tojo et al., 2017). In the case of propionate, butyrate, and valerate, high acetate concentrations might further inhibit their consumption (see Batstone et al. (2002) and Capson-Tojo et al. (2017) for a deeper discussion on AD thermodynamics). As the modified ADM1 included SAO and HM, it was able to predict high H_2 concentrations and partial pressures in the reactor, thus accurately predicting VFA accumulation. The default ADM1 could not predict an AD system dominated via SAO and HM, and thus could not predict the consequent high H_2 concentrations and the resulting VFA accumulation. Therefore, to represent the VFA profiles, the calibration procedure decreased the k_La value in the default ADM1 to values allowing the high H_2 concentrations required. The k_La estimated by the default ADM1 was much lower than the one obtained with the modified ADM1 (0.087 and 0.390 d^{-1}, respectively). The low k_La value resulted in the accumulation of, not only H_2, but also CH_4, reason why the methane production rates could not be predicted by the default ADM1.

The phenomena described above can also explain the resulting k_m values. Regarding acetate, the default ADM1 needed a high $k_{m,ac}$ value of 10.7 g COD·g COD^{-1}·d^{-1}, while the value in the modified ADM1 was 1.30 g COD·g COD^{-1}·d^{-1}, as SAO was the dominant acetate-consuming pathway. AM was irrelevant in the modified model (see Fig. 3B), leading to biased values of $k_{m,ac}$. Similarly, the less pronounced H_2-induced inhibition predicted by the default model (due to lower H_2 concentrations as HM was marginal) resulted in a very low value of k_m for

propionate uptake (2.93 g COD·g COD^{-1}·d^{-1}, far from literature values) to reproduce the propionate accumulation observed experimentally. In contrast, the k_m for propionate uptake in the modified ADM1 (19.2 g COD·g COD^{-1}·d^{-1}) was within ranges commonly reported in the literature (Batstone et al., 2002). Regarding the H_2 uptake rates, the values in the modified ADM1 allowed a simultaneous, syntrophic growth of hydrogenotrophic archaea and SAO (Fig. 3B). The higher values of k_m in the default ADM1 resulted in an initial fast H_2 consumption, followed by the death of hydrogenotrophic archaea (Fig. 3A). This allowed to reduce the initial H_2 concentrations to values where there was no VFA accumulation. Nevertheless, as in the default ADM1 SAO did not occur, less H_2 was predicted than in the modified ADM1, which jeopardised the simultaneous representation of methane production rates and VFA profiles.

Butyrate and valerate uptake were separated into two different processes in the modified ADM1, aiming at accurately representing their profiles. This strategy allowed setting different uptake dynamics for each clade, as it was obvious from the experimental data that they had different dynamics (more butyrate was initially generated than valerate, butyrate was produced faster, and valerate consumption was slower). Despite these efforts, both models failed to accurately predict the valerate profile (R^2 of 0.74-0.82). The most plausible explanation is that other processes were taking place, affecting both butyrate and valerate concentrations. Several biological reactions involve these compounds as substrate or products, and relevant processes such as chain elongation are known to occur during fermentation or AD of FW (Capson-Tojo et al., 2018b). Nonetheless, the low concentrations of valerate during FW AD (< 5% of the total COD as products) justify the omission of other involved processes. If an accurate prediction of valerate concentrations in the future is needed, further research should be carried out.

Another difference between the default and the modified ADM1 is the method used for FAN quantification and FAN-related inhibition. These differences affected the predicted pH profiles (more accurate in the modified ADM1), and thus also the FAN concentrations, which the

default ADM1 underestimated by up to 55% (Figs. 3C and 3D). This underestimated FAN concentrations imply that, under a correct FAN calculation, the calibrated value of $K_{I,NH3}$ in the default ADM1 would be considerably higher than those presented in Table 2, leading to even less realistic values. It must be considered that these differences between the predicted FAN concentrations are not only a consequence of the different pH values, but also of including the ionic strength in the FAN concentration estimation procedure.

3.2. Model application: using the modified ADM1 to explain the effect of AD additives

Carbon conductive materials have been reported to enhance the performance of AD reactors, particularly in FAN-rich digesters (Barua and Dhar, 2017). Improvements due to GAC addition have been related to: (i) allowing direct interspecies electron transfer (DIET) (Barua and Dhar, 2017); (ii) the formation of biofilms on its surface (Fagbohungbe et al., 2017); (iii) the sorption of inhibitors onto its surfaces (Fagbohungbe et al., 2017); and (iv) an increased buffering capacity (Barua and Dhar, 2017). Bioprocess modelling has never been used to increase our understanding on this topic, likely because available models did not include some of the relevant metabolic pathways occurring in the reactors.

The modified and default ADM1s were calibrated over experiments supplemented with GAC (after inoculum adaptation in sequential batch reactors). The calibration and modelling results are shown in Table 3 and Fig. 4, respectively. The modified ADM1 was able to represent the total VFA, acetate, and propionate profiles, and the methane production rates (R^2 values from parity plots of 0.93-0.99). As previously, butyrate and valerate concentrations were predicted less accurately. The default ADM1 showed the same limitations found with the control reactor, with barely any methane production (R^2 of 0.16) due to an extremely low k_La value. For both models, the corresponding FAN inhibition constants and predicted biomass concentrations (not shown, similar to those in Fig. 3) confirmed the predominant pathways described for the control reactor, *i.e.* SAO and HM being dominant in the modified ADM1 and AM in the default ADM1

422 (see Table 3 for inhibitory constants).

423 The calibration results (Table 3) show that GAC addition significantly enhanced the H_2 uptake
424 kinetics ($k_{m,H2}$ of 4.7 g COD·g $COD^{-1}·d^{-1}$ in the control reactor and of 24 g COD·g $COD^{-1}·d^{-1}$
425 in the GAC dosed reactor), which resulted in a faster uptake of the other VFAs due to a lower
426 H_2 partial pressure. The kinetics of SAO, propionate, butyrate, or valerate uptake were not
427 directly enhanced by GAC addition. These results suggest that the improvement observed in
428 AD performance after GAC addition is mainly due to a faster HM kinetics. This can be a
429 consequence of biofilm formation onto the GAC particles, thus favouring syntrophic
430 interactions. Another explanation could be the occurrence of DIET, which is a faster electron
431 transfer mechanism than mediated transport. As single electrons are not a state variable in the
432 model, DIET would simply be translated in the model as a faster HM process. These
433 mechanisms have been further discussed in Capson-Tojo et al. (2018a). Opposed to these
434 findings, the calibration results using the default ADM1 (Table 3) would explain these
435 enhancements via increasing the AM and SPO rates. As microbial community analyses showed
436 that the relative abundance of AM in the reactors was negligible, the default ADM1 would have
437 led to misleading conclusions.

438 These results show that the modified ADM1 can be applied to further understand the underlying
439 processes governing FW AD. The application shown here indicates that the modified ADM1
440 can be used to explain the positive effects that AD additives have on the process kinetics,
441 allowing to identify the processes that are more significantly affected.

442 *3.3. Comparison of the obtained parameters with literature values*

443 The parameters from the default ADM1 agree with those reported by other studies modelling
444 FW without including SAO. Zhao et al. (2019) targeted k_{dec}, k_{dis}, $k_{hyd,ch}$, $k_{m,ac}$, and $K_{S,ac}$ for
445 calibration due to their significant influence on methane production. The recommended
446 calibration values were 0.001 g COD·g $COD^{-1}·d^{-1}$, 0.16 g COD·g $COD^{-1}·d^{-1}$, 3 g COD·g

447 $COD^{-1} \cdot d^{-1}$, 1 g COD·g $COD^{-1} \cdot d^{-1}$, and 0.23 mg $COD \cdot L^{-1}$, respectively. The values of these
448 parameters for both models (presented in Tables 2 and 3; $k_{m,ac}$, and $K_{S,ac}$ only for the default
449 ADM1) are within the ballpark of those previously reported, confirming their applicability (see
450 values from the control reactor for less biased comparisons). The obtained k_{dis} values are also
451 close to those recommended in the ADM1 for food waste, of 0.41 d^{-1} (Batstone et al., 2002).
452 Regarding inhibitory parameters, values of $K_{I,NH3}$ up to 0.0028 M have been used for AD of the
453 organic fraction of municipal solid waste (Pastor-Poquet et al., 2019). As the values obtained
454 in this article (up to 0.0035 M), a $K_{I,NH3}$ of 0.0028 M is much higher than the common inhibitory
455 limit applied in the default ADM1 (0.0018 M). However, it must be considered that the default
456 ADM1 was designed for modelling AD of dilute sewage sludge (TS <5%) from wastewater
457 treatment plants, with lower FAN concentrations, thus representing microbial communities
458 unadapted to high FAN concentrations. The corresponding inhibitory limit to be used for FAN-
459 adapted processes (applied in our modified model) has been estimated around 0.0057 M
460 (corresponding to values of $4.3 \cdot 10^{-4}$ M and 0.0109 M for $K_{I,NH3,min,acet}$ and $K_{I,NH3,max,acet}$ in the
461 threshold function) (Capson-Tojo et al., 2020).
462 The results from sensitivity analyses and model calibrations carried out in previous publications
463 including SAO also agree with those presented in Tables 2 and 3 for the modified ADM1
464 (Montecchio et al., 2017; Rivera-Salvador et al., 2014). In previous publications, the kinetic
465 parameters (*e.g.* uptake rates) related to SAO and HM were found to be relevant (Montecchio
466 et al., 2017; Rivera-Salvador et al., 2014). For comparison purposes, Table 4 shows the values
467 of the uptake rates for acetate-uptake related processes (*i.e.* AM and SAO) and for HM, from
468 the literature and from this study. It must be considered that the data used in this work (and in
469 most of the studies presented in Table 4) was obtained from batch reactors. Therefore, the initial
470 biomass concentrations influenced to some extent the values of the obtained kinetic parameters.
471 It is important to consider that most previous AD models including SAO omitted AM, thus

excluding potential interactions between competing pathways (Montecchio et al., 2017; Rivera-Salvador et al., 2014). The modified ADM1 presented here considers both AM and SAO, which means that microbial competitions and shifts can be modelled by considering environmental factors (*e.g.* FAN concentration). To the best of our knowledge, only Wett et al. (2014) implemented both AM and SAO simultaneously, but they did not discuss competitions between them, neither their inhibition under different conditions. In practice, Wett et al. (2014) virtually omitted AM, since the k_m values were extremely low (0.3 kg COD·kg $COD^{-1}·d^{-1}$, see Table 4).

3.4. Implications for industrial application and further model development

This work shows that to properly model FW AD, key modifications must be made to the default ADM1 (*i.e.* including SAO and the impact of ionic strength on ion speciation). These modifications are important for the accurate prediction of the performances of digesters treating FW, which otherwise could not be achieved (*e.g.* inaccurate biogas production rates and/or acetate and propionate concentrations in the digesters by the default ADM1). In FW AD, VFAs accumulation is responsible for low performance, or even reactor failure. Their accurate prediction is crucial to understand the behaviour of these systems, to improve digester design, and to better assess mitigation strategies.

The accurate representation of methane and the VFA profiles has direct implications for optimisation of operational parameters (*e.g.* loading rates and retention times), for simulating scenarios with different co-substrates (*e.g.* predicting the impact of introducing a new waste stream into a territorial digester), for predicting AD inhibition scenarios, and for optimising the co-substrate proportions. These improvements will result in an enhanced waste valorisation. Including competing pathways (*e.g.* AM or SAO as dominant acetate-consuming pathway) has further practical benefits, since it allows: (i) to account for microbial adaptation without the need of continuous model recalibration; and (ii) to model microbial shifts (*e.g.* from dominant AM to HM), which could potentially be used to move away from the traditional operational

approach of stopping the reactor feed at minimal VFA increases. We consider that the benefits of implementing the modified ADM1 presented here outweigh the minor increase in model complexity. We recommend the application of the modified ADM1 for any AD system where it is suspected that AM might be inhibited due to high FAN concentrations (*i.e.* over 340 mg FAN-N·L^{-1}, based on Capson-Tojo et al. (2020)). The application of this model is not only restricted to FW AD, but can also be extended to any FAN-rich reactor, such as manure digesters. Further work should focus on calibration and validation of the modified ADM1 with continuous experiments, testing microbial acclimation to FAN and microbial shifts (*e.g.* from AM to HM).

AD models (high-solids models in particular) should account for the non-ideal behaviour of the solution. Further modifications to include activity corrections for chemical species other than FAN, or to consider ion pairing, would allow to: (i) improve the pH and model performance predictions (Solon et al., 2015); (ii) to accurately predict inhibition by other compounds (*e.g.* H_2S) (Durán et al., 2020; Patón et al., 2018); and (iii) to model the precise chemical speciation and complexation of relevant elements (*e.g.* P, S or Fe) (Flores-Alsina et al., 2016). Although non-ideality considerations are commonly considered by using the Debye-Hückel equation, fully defined comprehensive chemistry engines (*e.g.* PHREEQC or MINTEQA2) could also be integrated with AD models (Durán et al., 2020). Ion pairing and activity corrections could be coupled to a model considering TE complexation and precipitation, which would be particularly relevant if TEs are dosed in the digesters (Frunzo et al., 2019; Maharaj et al., 2019). Another potential modification could be to consider the variable TS contents in the reactors. As explained in Pastor-Poquet et al. (2018), the TS content can change in high-solids AD reactors due to the conversion of solid organics into biogas (up to around 10% with municipal solid waste as substrate). Consequently, the concentrations of soluble compounds and solids in the reactors can be affected. This effect was not considered in this work because the change in

volume from the start to the end of the experiments was considered negligible under the working conditions (estimated at 3-5% reactor volume loss).

The accurate prediction of FAN inhibitory limits is relevant, as it allows the compare the obtained values with those from the literature, and to obtain accurate limits for different predominant microbial communities. Furthermore, applying a more realistic model can help to provide a better understanding of FAN inhibition in anaerobic systems and to better predict microbial community shifts due to inhibition. Proper modelling of FAN-rich systems (including accurate inhibition limits) would improve the predictions of acetic and propionic acid profiles, which in turn could be used to better understand the impact of additives (*e.g.* GAC) on AD. This will not only assist in optimising the dosage and characteristics of these additives but will also aid to find other alternatives.

4. Conclusions

Results showed that the modified ADM1 is a suitable approach to model FW AD. The modified ADM1 was able to represent the methane production rates and the VFA profiles simultaneously, which could not be achieved with the default ADM1. The modified model also predicted the predominant acetate-consuming and methane-producing microbial clades, with SAO and HM being dominant. A modified Davies equation accurately estimated FAN concentrations, which improved pH predictions and provided better estimates for inhibition limits. Finally, the modified model showed that the addition of GAC enhances FW AD by improving the HM kinetics.

E-supplementary material

E-supplementary material for this work can be found in the online version of the paper.

Acknowledgements

Gabriel Capson-Tojo is grateful to the Xunta de Galicia for his postdoctoral fellowship (ED481B-2018/017). Sergi Astals is thankful to the Spanish Ministry of Science, Innovation and Universities for his Ramon y Cajal fellowship (RYC-2017-22372). Ángel Robles is grateful for the support from the Spanish Ministry of Science and Innovation and the Partnership for Research and Innovation in the Mediterranean Area (Grant PCI2020-112218).

References

1. Angelidaki, I., Alves, M.M., Bolzonella, D., Borzacconi, L., Campos, J.L., Guwy, A.J., Kalyuzhnyi, S., Jenicek, P., Van Lier, J.B., 2009. Defining the biomethane potential (BMP) of solid organic wastes and energy crops: a proposed protocol for batch assays.
2. APHA, 2017. Standard Methods for the Examination of Water and Wastewater. American Public Health Association, Washington, DC.
3. Appels, L., Baeyens, J., Degrève, J., Dewil, R., 2008. Principles and potential of the anaerobic digestion of waste-activated sludge. Prog. Energy Combust. Sci. 34, 755–781.
4. Astals, S., Esteban-Gutiérrez, M., Fernández-Arévalo, T., Aymerich, E., García-Heras, J.L., Mata-Alvarez, J., 2013. Anaerobic digestion of seven different sewage sludges: A biodegradability and modelling study. Water Res. 47, 6033–6043.
5. Astals, S., Peces, M., Batstone, D.J., Jensen, P.D., Tait, S., 2018. Characterising and modelling free ammonia and ammonium inhibition in anaerobic systems. Water Res. 143, 127–135.
6. Banks, C.J., Chesshire, M., Stringfellow, A., 2008. A pilot-scale trial comparing mesophilic and thermophilic digestion for the stabilisation of source segregated kitchen waste. Water Sci. Technol. 58, 1475–1481.
7. Banks, C.J., Zhang, Y., Jiang, Y., Heaven, S., 2012. Trace element requirements for stable food waste digestion at elevated ammonia concentrations. Bioresour. Technol. 104, 127–135.
8. Barua, S., Dhar, B.R., 2017. Advances Towards Understanding and Engineering Direct Interspecies Electron Transfer in Anaerobic Digestion. Bioresour. Technol. 244, 698–707.
9. Batstone, D.J., Keller, J., Angelidaki, I., Kalyuzhny, S. V, Pavlostathis, S.G., Rozzi, A., Sanders, W.T.M., Siegrist, H., Vavilin, V.A., 2002. Anaerobic digestion model no. 1 (ADM1). IWA Publishing.
10. Campolongo, F., Cariboni, J., Saltelli, A., 2007. An effective screening design for sensitivity analysis of large models. Environ. Model. Softw. 22, 1509–1518.
11. Capson-Tojo, G., Moscoviz, R., Astals, S., Robles, A., Steyer, J.-P., 2020. Unraveling the literature chaos around free ammonia inhibition in anaerobic digestion. Renew. Sustain. Energy Rev. 117, 109487.
12. Capson-Tojo, G., Moscoviz, R., Ruiz, D., Santa-Catalina, G., Trably, E., Rouez, M., Crest, M., Steyer, J.-P., Bernet, N., Delgenès, J.-P., Escudié, R., 2018a. Addition of granular activated carbon and trace elements to favor volatile fatty acid consumption during anaerobic digestion of food waste. Bioresour. Technol. 260, 157–168.

13. Capson-Tojo, G., Rouez, M., Crest, M., Steyer, J.-P., Delgenès, J.-P., Escudié, R., 2016. Food waste valorization via anaerobic processes: a review. Rev. Environ. Sci. Bio/Technology 15, 499–547.
14. Capson-Tojo, G., Ruiz, D., Rouez, M., Crest, M., Steyer, J.-P., Bernet, N., Delgenès, J.-P., Escudié, R., 2017. Accumulation of propionic acid during consecutive batch anaerobic digestion of commercial food waste. Bioresour. Technol. 245, 724–733.
15. Capson-Tojo, G., Trably, E., Rouez, M., Crest, M., Bernet, N., Steyer, J.-P., Delgenès, J.-P., Escudié, R., 2018b. Cardboard proportions and total solids contents as driving factors in dry co-fermentation of food waste. Bioresour. Technol. 248, 229–237.
16. De Vrieze, J., Saunders, A.M., He, Y., Fang, J., Nielsen, P.H., Verstraete, W., Boon, N., 2015. Ammonia and temperature determine potential clustering in the anaerobic digestion microbiome. Water Res. 75, 312–323.
17. Dubois, M., Gilles, K.A., Hamilton, J.K., Rebers, P.A., Smith, F., 1956. Colorimetric Method for Determination of Sugars and Related Substances. Anal. Chem. 28, 350–356.
18. Durán, F., Robles, Á., Giménez, J.B., Ferrer, J., Ribes, J., Serralta, J., 2020. Modelling the anaerobic treatment of sulfate-rich urban wastewater: application to AnMBR technology. Water Res. 184, 116133.
19. Fagbohungbe, M.O., Herbert, B.M.J., Hurst, L., Ibeto, C.N., Li, H., Usmani, S.Q., Semple, K.T., 2017. The challenges of anaerobic digestion and the role of biochar in optimizing anaerobic digestion. Waste Manag. 61, 236–249.
20. Flores-Alsina, X., Solon, K., Kazadi Mbamba, C., Tait, S., Gernaey, K. V., Jeppsson, U., Batstone, D.J., 2016. Modelling phosphorus (P), sulfur (S) and iron (Fe) interactions for dynamic simulations of anaerobic digestion processes. Water Res. 95, 370–382.
21. Frunzo, L., Fermoso, F.G., Luongo, V., Mattei, M.R., Esposito, G., 2019. ADM1-based mechanistic model for the role of trace elements in anaerobic digestion processes. J. Environ. Manage. 241, 587–602.
22. Galí, A., Benabdallah, T., Astals, S., Mata-Alvarez, J., 2009. Modified version of ADM1 model for agro-waste application. Bioresour. Technol. 100, 2783–2790.
23. Hafner, S.D., Bisogni, J.J., 2009. Modeling of ammonia speciation in anaerobic digesters. Water Res. 43, 4105–4114.
24. Hao, L., Michaelsen, T.Y., Singleton, C.M., Dottorini, G., Kirkegaard, R.H., Albertsen, M., Nielsen, P.H., Dueholm, M.S., 2020. Novel syntrophic bacteria in full-scale anaerobic digesters revealed by genome-centric metatranscriptomics. ISME J. 14, 906–918.
25. Jiang, Y., Banks, C., Zhang, Y., Heaven, S., Longhurst, P., 2017. Quantifying the percentage of methane formation via acetoclastic and syntrophic acetate oxidation pathways in anaerobic digesters. Waste Manag. 71, 749–756.
26. Karthikeyan, O.P., Visvanathan, C., 2013. Bio-energy recovery from high-solid organic substrates by dry anaerobic bio-conversion processes: a review. Rev. Environ. Sci. Bio/Technology 12, 257–284.
27. Koch, K., Helmreich, B., Drewes, J.E., 2015. Co-digestion of food waste in municipal wastewater treatment plants: Effect of different mixtures on methane yield and hydrolysis rate constant. Appl. Energy 137, 250–255.
28. Maharaj, B.C., Mattei, M.R., Frunzo, L., Hullebusch, E.D. va., Esposito, G., 2019. ADM1 based mathematical model of trace element complexation in anaerobic digestion processes. Bioresour. Technol. 253–259.
29. Montecchio, D., Astals, S., Di Castro, V., Gallipoli, A., Gianico, A., Pagliaccia, P., Piemonte, V., Rossetti, S., Tonanzi, B., Braguglia, C.M., 2019. Anaerobic co-digestion of

food waste and waste activated sludge: ADM1 modelling and microbial analysis to gain insights into the two substrates' synergistic effects. Waste Manag. 97, 27–37.
30. Montecchio, D., Esposito, G., Gagliano, M.C., Gallipoli, A., Gianico, A., Braguglia, C.M., 2017. Syntrophic acetate oxidation during the two-phase anaerobic digestion of waste activated sludge: Microbial population, Gibbs free energy and kinetic modelling. Int. Biodeterior. Biodegrad. 125, 177–188.
31. Morris, M., 1991. Factorial sampling plans for preliminary computational experiments. Technometrics 33, 239–245.
32. Moscoviz, R., de Fouchécour, F., Santa-Catalina, G., Bernet, N., Trably, E., 2017. Cooperative growth of Geobacter sulfurreducens and Clostridium pasteurianum with subsequent metabolic shift in glycerol fermentation. Sci. Rep. 7, 44334.
33. Motte, J.-C., Escudié, R., Beaufils, N., Steyer, J.-P., Bernet, N., Delgenès, J.-P., Dumas, C., 2014. Morphological structures of wheat straw strongly impacts its anaerobic digestion. Ind. Crops Prod. 52, 695–701.
34. Motte, J.-C., Trably, E., Escudié, R., Hamelin, J., Steyer, J.-P., Bernet, N., Delgenes, J.-P., Dumas, C., 2013. Total solids content: a key parameter of metabolic pathways in dry anaerobic digestion. Biotechnol. Biofuels 6, 164.
35. Pastor-Poquet, V., Papirio, S., Steyer, J.P., Trably, E., Escudié, R., Esposito, G., 2019. Modelling non-ideal bio-physical-chemical effects on high-solids anaerobic digestion of the organic fraction of municipal solid waste. J. Environ. Manage. 238, 408–419.
36. Pastor-Poquet, V., Papirio, S., Steyer, J.P., Trably, E., Escudié, R., Esposito, G., 2018. High-solids anaerobic digestion model for homogenized reactors. Water Res. 142, 501–511.
37. Patón, M., González-Cabaleiro, R., Rodríguez, J., 2018. Activity corrections are required for accurate anaerobic digestion modelling. Water Sci. Technol. 77, 2057–2067.
38. Poggio, D., Walker, M., Nimmo, W., Ma, L., Pourkashanian, M., 2016. Modelling the anaerobic digestion of solid organic waste - Substrate characterisation method for ADM1 using a combined biochemical and kinetic parameter estimation approach. Waste Manag. 53, 40–54.
39. Rajagopal, R., Massé, D.I., Singh, G., 2013. A critical review on inhibition of anaerobic digestion process by excess ammonia. Bioresour. Technol. 143, 632–641.
40. Rathnasiri, P.G., 2016. Dynamic Modelling and Simulation of Pilot Scale Anaerobic Digestion Plant Treating Source Separated Food Waste and Effect of Recycling Sludge. Procedia Environ. Sci. 35, 740–748.
41. Regmi, P., Miller, M., Jimenez, J., Stewart, H., Johnson, B., Amerlinck, Y., Volcke, E.I.P., Arnell, M., García, P.J., Maere, T., Torfs, E., Vanrolleghem, P.A., Miletić, I., Rieger, L., Schraa, O., Samstag, R., Santoro, D., Snowling, S., Takács, I., 2019. The future of WRRF modelling - Outlook and challenges. Water Sci. Technol. 79, 3–14.
42. Rivera-Salvador, V., López-Cruz, I.L., Espinosa-Solares, T., Aranda-Barradas, J.S., Huber, D.H., Sharma, D., Toledo, J.U., 2014. Application of Anaerobic Digestion Model No. 1 to describe the syntrophic acetate oxidation of poultry litter in thermophilic anaerobic digestion. Bioresour. Technol. 167, 495–502.
43. Robles, A., Ruano, M. V., Ribes, J., Seco, A., Ferrer, J., 2014. Global sensitivity analysis of a filtration model for submerged anaerobic membrane bioreactors (AnMBR). Bioresour. Technol. 158, 365–373.
44. Rosen, C., Jeppsson, U., 2006. Aspects on ADM1 Implementation within the BSM2 Framework. Tech. Rep. 1–37.

45. Solon, K., Flores-Alsina, X., Mbamba, C.K., Volcke, E.I.P., Tait, S., Batstone, D., Gernaey, K. V., Jeppsson, U., 2015. Effects of ionic strength and ion pairing on (plant-wide) modelling of anaerobic digestion. Water Res. 70, 235–245.
46. Stumm, W., Morgan, J.J., 1996. Aquatic Chemistry: Chemical Equilibria and Rates in Natural Waters, 3rd ed. John Wiley & Sons.
47. Weinrich, S., Nelles, M., 2021. Systematic simplification of the Anaerobic Digestion Model No. 1 (ADM1) – Model development and stoichiometric analysis. Bioresour. Technol. 333.
48. Wett, B., Takács, I., Batstone, D., Wilson, C., Murthy, S., 2014. Anaerobic model for high-solids or high-temperature digestion - Additional pathway of acetate oxidation. Water Sci. Technol. 69, 1634–1640.
49. Zhao, X., Li, L., Wu, D., Xiao, T., Ma, Y., Peng, X., 2019. Modified Anaerobic Digestion Model No. 1 for modeling methane production from food waste in batch and semi-continuous anaerobic digestions. Bioresour. Technol. 271, 109–117.

Figure and table captions

Figure 1. Results of the sensitivity analysis of the control reactor for the five model outputs used for calibration (*i.e.* methane flow rate and concentrations of acetate, propionate, butyrate, and valerate). Results for both the (A-E) default ADM1 and the (F-J) modified ADM1 are presented.

Figure 2. Experimental data and modelling results corresponding to the methane production curves (Q_{CH4}) and the concentrations of acetate, propionate, butyrate, and valerate in the control reactor. Modelling results using the (A-F) default ADM1 and the (G-L) modified ADM1 are presented. The R^2 given correspond to parity plots.

Figure 3. Predicted biomass concentrations by (A) the default ADM1 and (B) the modified ADM1 with data from the control reactor. The (C) pH and (D) TAN and FAN concentrations predicted by both models are also shown.

Figure 4. Experimental data and modelling results corresponding to the methane production curves (Q_{CH4}) and the concentrations of acetate, propionate, butyrate, and valerate for the GAC-supplemented reactor. The modelling results for both the (A-F) modified ADM1 and the (G-L) default ADM1 are shown. The R^2 given correspond to parity plots.

Table 1. Main characteristics (average and standard deviations) of the food waste and the inoculum.

Table 2. Calibration results for the control reactor of the relevant parameters in the default and the modified ADM1. The results correspond to the control reactor (no additives supplied). The values from the ADM1 are given for mesophilic conditions (35 ºC).

Table 3. Calibration results for the control reactor and for reactors supplemented with granular activated carbon (GAC). The results from parameters deemed as relevant are shown for both the default and the modified ADM1.

Table 4. Values of uptake rates (k_m; kg COD·kg COD^{-1}·d^{-1}) related to acetate and hydrogen uptake from the literature and in this study.

Credit author statement

Conceptualization was performed by GC-T, SA and AR. GC-T and AR carried out methodology, software, and formal analysis. GC-T and SA wrote the original manuscript. GC-T, SA and AR carried out manuscript review and editing. Visualisation was performed by GCT.

All authors contributed to the article and approved the submitted version.

Declaration of interest statement

The authors do not have interests to declare.

Highlights

- The modified ADM1 improved the predicted methane and volatile fatty acids profiles
- The modified ADM1 enhanced free ammonia estimation and inhibition modelling
- The predominant metabolic pathways were adequately predicted
- k_La and k_{dis} were relevant parameters for accurate food waste digestion modelling
- Model results showed that granular activated carbon enhanced hydrogen uptake

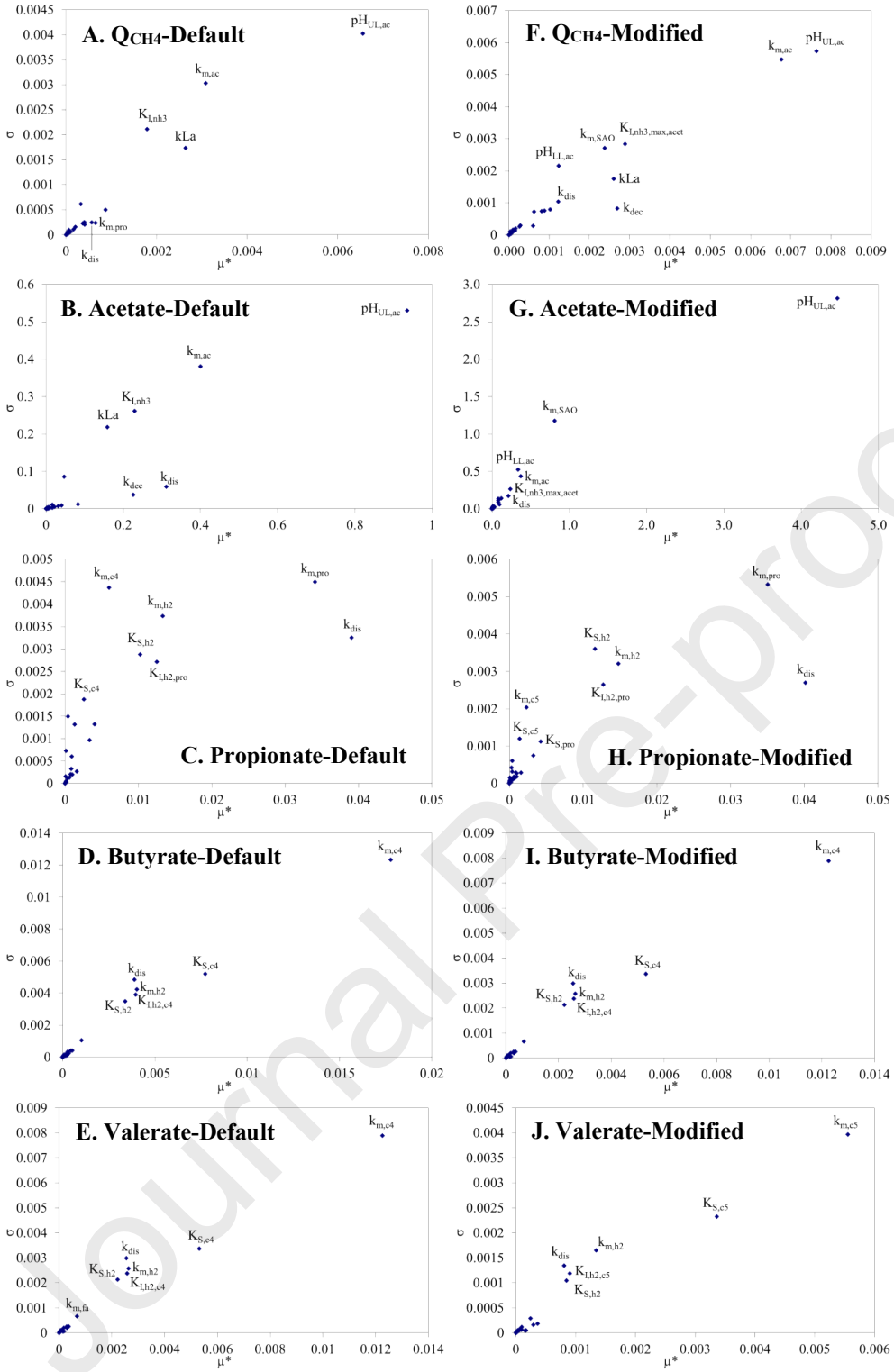

741

742 **Figure 1.** Results of the sensitivity analysis of the control reactor for the five model outputs
743 used for calibration (*i.e.* methane flow rate and concentrations of acetate, propionate, butyrate,
744 and valerate). Results for both the (A-E) default ADM1 and the (F-J) modified ADM1 are

745 presented.

746

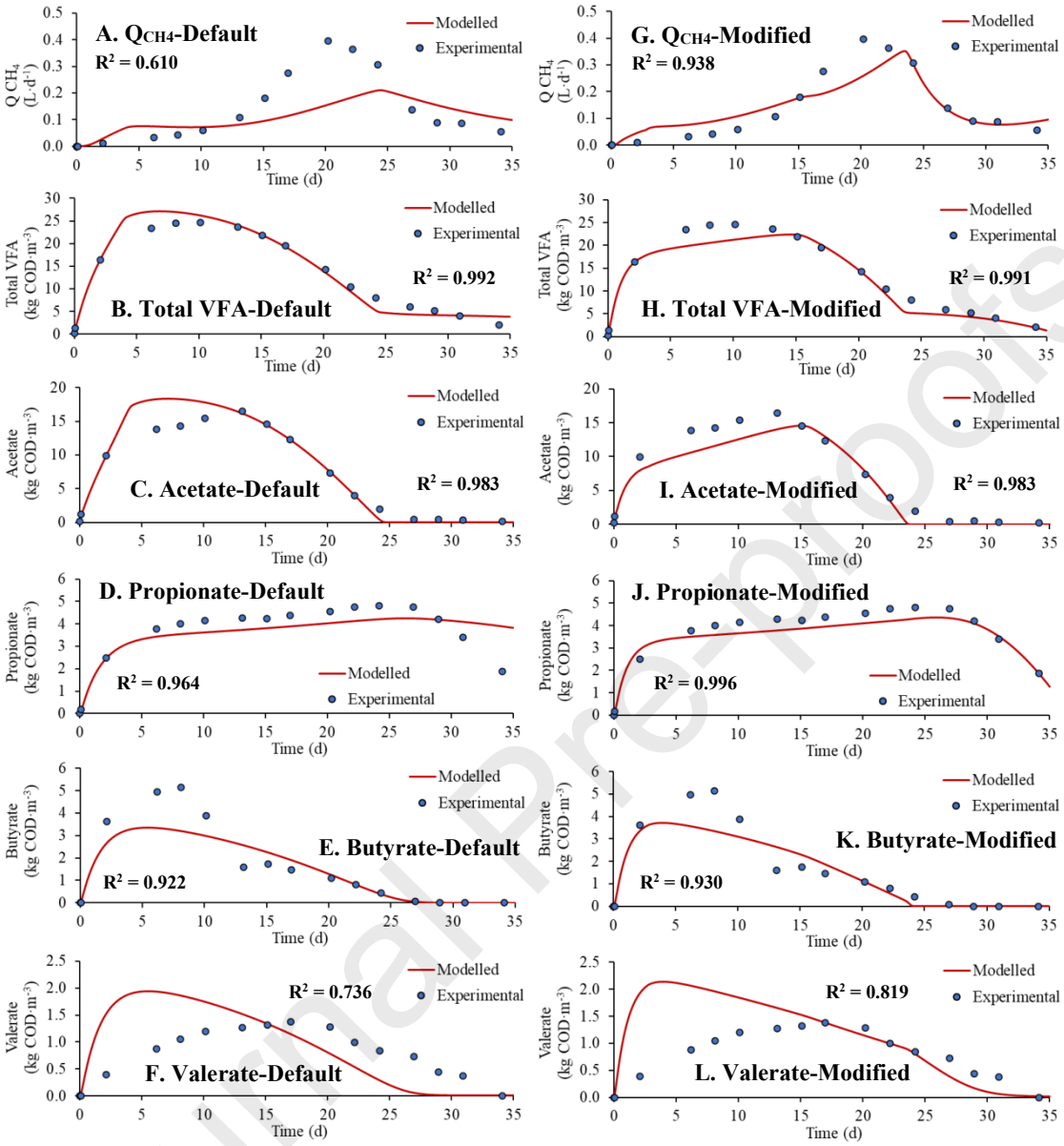

747

748 **Figure 2.** Experimental data and modelling results corresponding to the methane production
749 curves (Q_{CH4}) and the concentrations of acetate, propionate, butyrate, and valerate in the control
750 reactor. Modelling results using the (A-F) default ADM1 and the (G-L) modified ADM1 are
751 presented. The R^2 given correspond to parity plots.

752

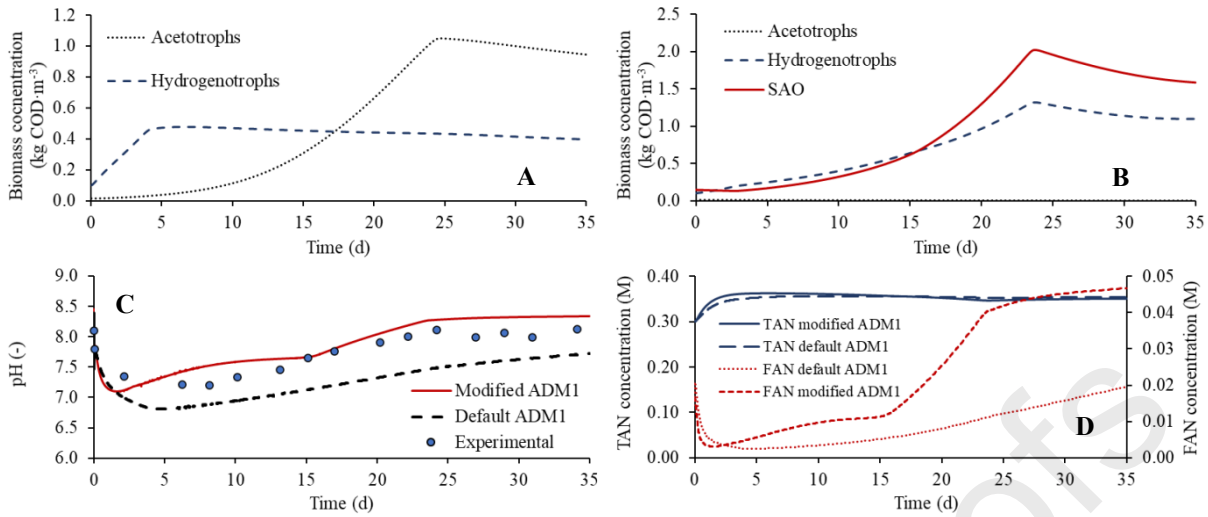

753

754 **Figure 3.** Predicted biomass concentrations by (A) the default ADM1 and (B) the modified

755 ADM1 with data from the control reactor. The (C) pH and (D) TAN and FAN concentrations

756 predicted by both models are also shown.

757

758

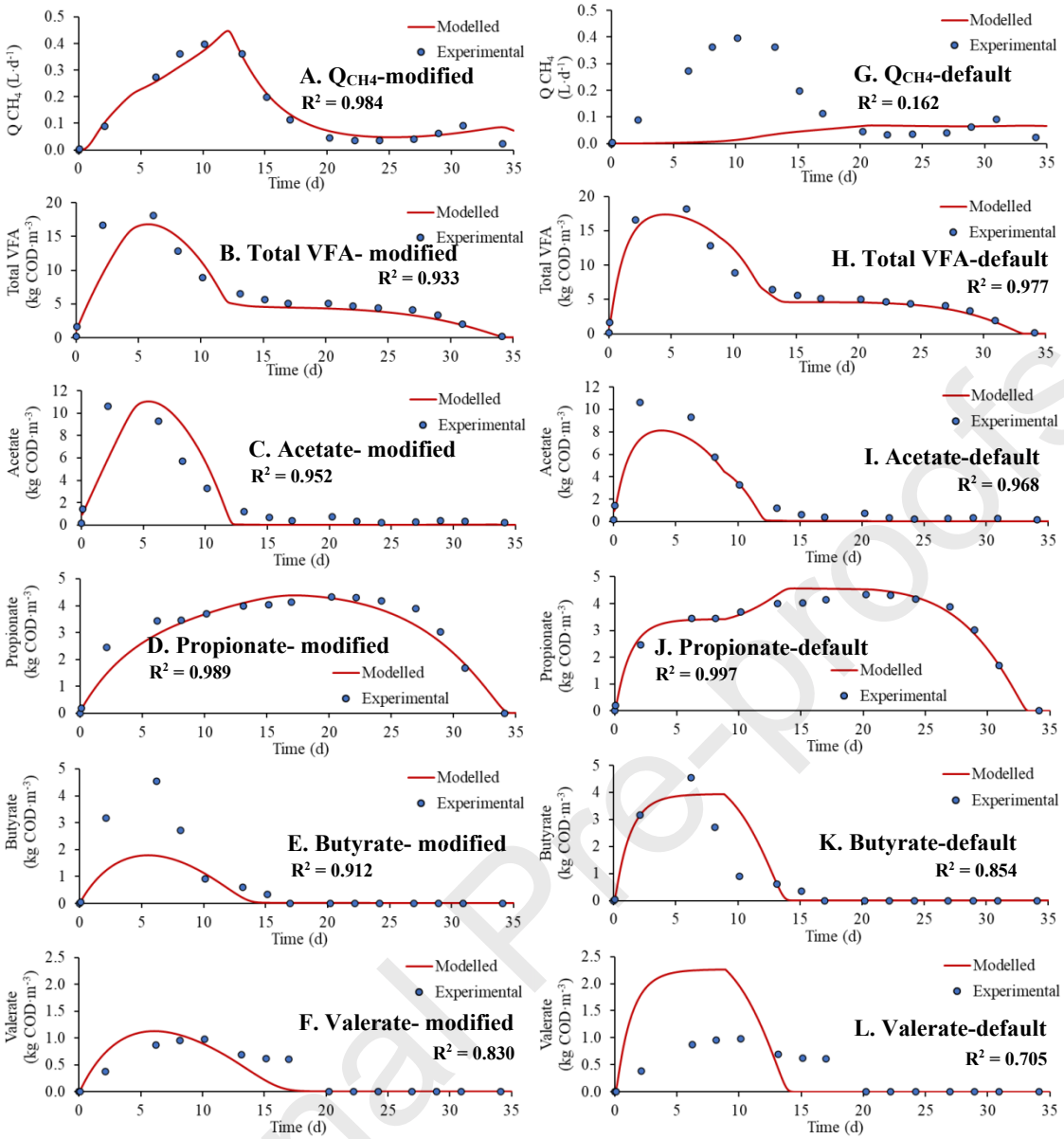

Figure 4. Experimental data and modelling results corresponding to the methane production curves (Q_{CH4}) and the concentrations of acetate, propionate, butyrate, and valerate for the GAC-supplemented reactor. The modelling results for both the (A-F) modified ADM1 and the (G-L) default ADM1 are shown. The R^2 given correspond to parity plots.

Table 1. Main characteristics (average and standard deviations) of the food waste and the inoculum.

Parameter	Food waste mixture	Inoculum

TS (%)	21.0 ± 0.36	6.14 ± 0.62
VS/TS (%)	90.3 ± 0.76	56.8 ± 3.56
Carbohydrates (g·kg TS^{-1})	618 ± 23	n.m.
Proteins (g·kg TS^{-1})	187 ± 10	n.m.
Lipids (g·kg TS^{-1})	121 ± 21	n.m.
BMPs (mL CH_4·g VS^{-1})	420 ± 5.28	n.m.
pH	5.02 ± 0.18	8.10 ± 0.10
TAN (g N·L^{-1})	0.90 ± 0.72	7.27 ± 0.51
TKN (g N·kg TS^{-1})	30.0 ± 1.64	n.m.

767 TS stands for total solids, VS for volatile solids, n.m. for "not measured", BMP for biochemical methane potential,
768 TAN for total ammonia nitrogen, and TKN for total Kjeldahl nitrogen
769

770
771 **Table 2.** Calibration results for the control reactor of the relevant parameters in the default and
772 the modified ADM1. The results correspond to the control reactor (no additives supplied). The
773 values from the ADM1 are given for mesophilic conditions (35 ºC).

Symbol	Parameter	Units	Default value	Source	Calibration results	
					Default ADM1	Modified ADM1
$\mathbf{k_{dis}}$	First order disintegration rate	g COD·g COD^{-1}·d^{-1}	0.5	(Batstone et al., 2002)	0.606	0.975
$\mathbf{k_La}$	Mass transfer coefficient	d^{-1}	200	(Rosen and Jeppsson, 2006)	0.087	0.390
$\mathbf{k_{m,ac}}$	Acetate uptake rate by methanogens	g COD·g COD^{-1}·d^{-1}	8	(Batstone et al., 2002)	10.74	1.292
$\mathbf{k_{m,pro}}$	Propionate uptake rate	g COD·g COD^{-1}·d^{-1}	13	(Batstone et al., 2002)	2.926	19.21
$\mathbf{k_{m,h2}}$	Hydrogen uptake rate	g COD·g COD^{-1}·d^{-1}	35	(Batstone et al., 2002)	21.82	4.684
$\mathbf{k_{m,c4}}$	Butyrate/valerate uptake rate [1]	g COD·g COD^{-1}·d^{-1}	20	(Batstone et al., 2002)	1.494	7.147
$\mathbf{k_{m,c5}}$	Valerate uptake rate	g COD·g COD^{-1}·d^{-1}	20	(Batstone et al., 2002)	-	2.894
$\mathbf{k_{m,SAO}}$	Acetate uptake rate by SAO	g COD·g COD^{-1}·d^{-1}	3.25	(Rivera-Salvador et al., 2014)	-	4.851
$\mathbf{k_{dec}}$	First order biomass decay rate	g COD·g COD^{-1}·d^{-1}	0.02	(Batstone et al., 2002)	0.015	0.039
$\mathbf{K_{S,c4}}$	Half saturation constant for butyrate/valerate [1]	mg COD·L^{-1}	0.2	(Batstone et al., 2002)	0.237	0.075
$\mathbf{K_{S,c5}}$	Half saturation constant for valerate	mg COD·L^{-1}	0.2	(Batstone et al., 2002)	-	0.390
$\mathbf{K_{S,h2}}$	Half saturation constant for hydrogen	mg COD·L^{-1}	$7\cdot10^{-6}$	(Batstone et al., 2002)	$3.2\cdot10^{-6}$	$1.2\cdot10^{-5}$
$\mathbf{K_{I,h2,c4}}$	H_2 50% inhibitory concentration for	mg COD·L^{-1}	$1\cdot10^{-5}$	(Batstone et al., 2002)	$1.9\cdot10^{-5}$	$2.9\cdot10^{-6}$

	butyrate/valerate uptake [1]					
$K_{I,h2,c5}$	H_2 50% inhibitory concentration for valerate uptake	mg COD·L^{-1}	$1 \cdot 10^{-5}$	(Batstone et al., 2002)	-	$8.4 \cdot 10^{-6}$
$K_{I,h2,pro}$	H_2 50% inhibitory concentration for propionate uptake	mg COD·L^{-1}	$3.5 \cdot 10^{-6}$	(Batstone et al., 2002)	$2.4 \cdot 10^{-7}$	$9.6 \cdot 10^{-7}$
$K_{I,NH3}$	NH_3 50% inhibitory concentration for acetate uptake by methanogens	M	0.0018	(Batstone et al., 2002)	0.0030	-
$K_{I,NH3,max,acet}$	FAN concentrations where inhibition of acetate uptake by methanogens is almost complete	M	0.0109	(Capson-Tojo et al., 2020)	-	0.011
$pH_{UL,ac}$	50% pH upper limit for acetotrophs	-	7	(Batstone et al., 2002)	7.12	-

SAO stands for syntrophic acetate oxidation and FAN for free ammonia nitrogen.
1. Valerate only in the default ADM1

Table 3. Calibration results for the control reactor and for reactors supplemented with granular activated carbon (GAC). The results from parameters deemed as relevant are shown for both the default and the modified ADM1.

Parameter	Units	Default ADM1		Modified ADM1	
		Control	GAC	Control	GAC
k_{dis}	g COD·g COD^{-1}·d^{-1}	0.606	0.802	0.975	0.236
$k_{m,ac}$	g COD·g COD^{-1}·d^{-1}	10.74	14.68	1.291	3.864
$k_{m,pro}$	g COD·g COD^{-1}·d^{-1}	2.93	9.55	19.21	5.927
$k_{m,h2}$	g COD·g COD^{-1}·d^{-1}	21.8	1.75	4.684	24.295
$k_{m,c4}$	g COD·g COD^{-1}·d^{-1}	1.49	22.2	7.147	2.261
$k_{m,c5}$	g COD·g COD^{-1}·d^{-1}	-	-	2.894	1.945
$k_{m,SAO}$	g COD·g COD^{-1}·d^{-1}	-	-	4.851	3.125
k_{dec}	g COD·g COD^{-1}·d^{-1}	0.015	0.009	0.039	0.039
$K_{S,c4}$	mg COD·L^{-1}	0.237	0.389	0.075	0.138
$K_{S,c5}$	mg COD·L^{-1}	-	-	0.390	0.234
$K_{S,h2}$	mg COD·L^{-1}	$3.2 \cdot 10^{-6}$	$4.5 \cdot 10^{-6}$	$1.2 \cdot 10^{-5}$	$7.2 \cdot 10^{-6}$
$K_{I,h2,c4}$	mg COD·L^{-1}	$1.9 \cdot 10^{-5}$	$1.1 \cdot 10^{-5}$	$2.9 \cdot 10^{-6}$	$1.5 \cdot 10^{-5}$
$K_{I,h2,c5}$	mg COD·L^{-1}	-	-	$8.4 \cdot 10^{-6}$	$1.9 \cdot 10^{-5}$
$K_{I,h2,pro}$	mg COD·L^{-1}	$2.4 \cdot 10^{-7}$	$4.0 \cdot 10^{-6}$	$9.6 \cdot 10^{-7}$	$1.0 \cdot 10^{-6}$
$K_{I,NH3}$	M	0.0030	0.0030	-	-
$K_{I,NH3,max,acet}$	M	-	-	0.011	0.010
$pH_{UL,ac}$	-	7.1	6.4	-	-
k_La	d^{-1}	0.087	0.016	0.390	0.374

781
782

783
784 **Table 4.** Values of uptake rates (k_m; kg COD·kg COD^{-1}·d^{-1}) related to acetate and hydrogen

785 uptake from the literature and in this study.

Reference	Substrate	SAO	AM	HM
(Rivera-Salvador et al., 2014)	Poultry litter	1.12	-	13
(Montecchio et al., 2017)	Sludge	7	-	70
(Wett et al., 2014)	Sludge	2.6	0.3	-
(Dwyer et al., 1988)	Butyrate and others	0.037-25.0	-	-
Default ADM1	-	-	16	35
This study (default ADM1)	FW	-	10.7-14.7	1.75-21.8
This study (modified ADM1)	FW	3.13-4.85	1.29-3.86	4.68-24.3

786 FW stands for food waste, SAO for syntrophic acetate oxidation, AM for acetoclastic methanogenesis, and HM
787 for hydrogenotrophic methanogenesis.
788
789 **Graphical abstract**

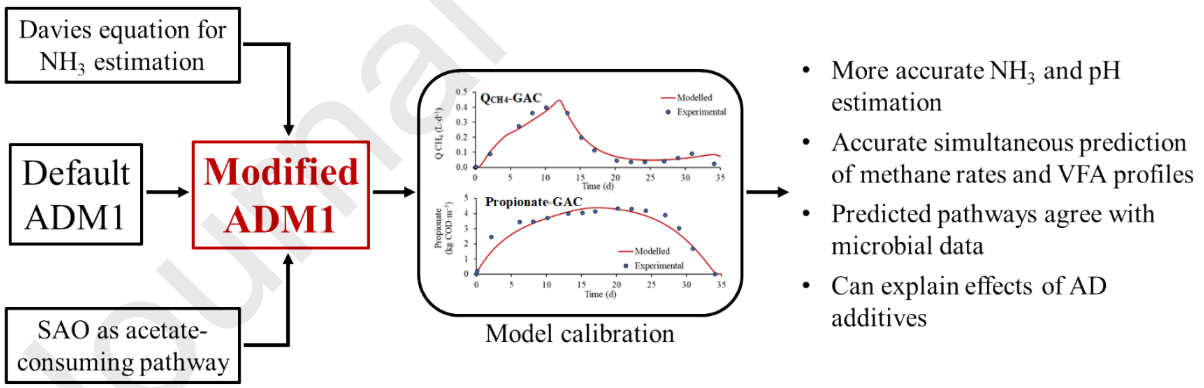

790

791

792